

KfK 5409
November 1994

Strength and Crack Growth Data for Fusion Relevant Ceramics

T. Fett
Institut für Materialforschung
Projekt Kernfusion

Kernforschungszentrum Karlsruhe

KERNFORSCHUNGSZENTRUM KARLSRUHE

Institut für Materialforschung

Projekt Kernfusion

KfK 5409

**Strength and crack growth data for
fusion relevant ceramics**

T. Fett

Kernforschungszentrum Karlsruhe GmbH, Karlsruhe

Als Manuskript gedruckt
Für diesen Bericht behalten wir uns alle Rechte vor

Kernforschungszentrum Karlsruhe GmbH
Postfach 3640, 76021 Karlsruhe

ISSN 0303-4003

Strength and crack growth data for fusion relevant ceramics

Abstract

Microwave heating is being considered as an external plasma heat source for fusion reactor systems. The window separating the reactor vacuum and the electron tube vacuum is heated up as a result of dielectric losses. The temperature gradients in the window cause thermal stresses. These stresses are responsible for failure and finite lifetimes of the ceramic materials. Three failure modes are of special interest: spontaneous failure, failure after subcritical crack growth and cyclic fatigue leading to a finite lifetime. A number of ceramic materials has been investigated. The results are reported by Weibull plots (strength), v -K-curves (subcritical crack growth) and $da/dN - \Delta K$ -curves (cyclic fatigue). For a number of materials also the fracture toughness K_{Ic} is given.

Festigkeit und Rißwachstumsdaten für fusionsrelevante Keramiken

Kurzfassung

Der Einsatz von Gyrotrons ist für Fusionsreaktoren geplant um das Plasma auf Zündbedingungen zu bringen. Zur Trennung des zum Betrieb des Gyrotron notwendigen Hochvakuums vom Plasma werden Keramikfenster eingesetzt. Aufgrund der dielektrischen Verluste heizt sich die Keramik auf und die sich einstellenden thermischen Spannungen können sofortiges oder zeitlich verzögertes Versagen des Fensters bewirken. Die dabei auftretenden Versagensarten sind: Erreichen der Kurzzeitfestigkeit, Versagen nach vorausgegangenem unterkritischem Rißwachstum sowie Versagen durch zyklische Ermüdung. Die Meßergebnisse an einer Reihe von Keramiken werden in Form von Weibull-Diagrammen (Festigkeit), v -K-Kurven (unterkritisches Rißwachstum) und $da/dN - \Delta K$ -Kurven (Ermüdung) mitgeteilt. Für einige der betrachteten Materialien werden zusätzlich Daten der Rißzähigkeit angegeben.

Contents

1. Introduction	1
<hr/>	
2. Materials and procedures	2
2.1 Materials	2
2.2 Spontaneous failure	3
2.2.1 Inert strength	3
2.2.2 Fracture toughness	3
2.3 Subcritical crack growth	4
2.3.1 Basic relations	4
2.3.2 Lifetime method for the determination of v-K-curves	4
2.4 Cyclic fatigue	7
2.4.1 Basic relations	7
2.4.2 Statistical procedure	8
2.4.3 Testing device	9
<hr/>	
3. Failure prediction	11
3.1 Spontaneous failure	11
3.2 Delayed failure	12
<hr/>	
4. Results	13
4.1 Parameters and references to curves in the Appendix	13
<hr/>	
5. References	17
<hr/>	
6. Appendix	18

1. Introduction

In the ceramic window of a gyrotron for fusion power applications thermal stresses occur due to the dielectric losses. These stresses are responsible for failure and finite lifetimes of the ceramic materials. The most important failure modes for temperatures below the creep region are

1. spontaneous failure,
2. subcritical crack growth under static load,
3. cyclic fatigue.

Spontaneous failure occurs when the stress applied reaches the inert strength of the material or, in terms of fracture mechanics, when the stress intensity factor K_I of the most severe crack in a component reaches or exceeds the fracture toughness K_{Ic} .

Delayed failure may be caused either by **subcritical crack growth**, governed by the actual stress intensity factor K_I , or by **crack propagation under cyclic load**, governed by the stress intensity factor range ΔK and probably the R-ratio defined as the ratio of minimum and maximum K-values. Therefore, the failure-relevant material data are above all the strength data expressed by the Weibull parameters σ_0 and m , and the parameters for quasi static and cyclic crack growth. These values characterise the qualification of a candidate material from the mechanical point of view. If the number of cycles is not excessively high, the failure behaviour can be characterised sufficiently by the inert strength and the subcritical crack-growth relation.

The aim of this report is to provide strength data as well as subcritical crack growth data (and cyclic fatigue data, if available) for several polycrystalline ceramic materials such as Al_2O_3 , AlN , $Al_2O_3 + ZrO_2$ and *sapphire*. The materials investigated are listed in Table 1.

2. Materials and procedures

2.1 Materials

Several fusion-relevant ceramics were investigated. In the following table the tests are listed:

Number	Material	Manufacturer or reference	Strength	K_{Ic}	SCG	Fatigue
I	Al_2O_3 99.99%	Ceraten	x		x	
II	Al_2O_3 >99.9%	Metoxit	x	x	x	
III	Al_2O_3 >99.9%	Metoxit	x	x	x	
IV	Al_2O_3 >99.9%	Metoxit, Thayngen	x	x	x	
V	Al_2O_3 99.7%	Feldmühle	x	x	x	
VI	Al_2O_3 99.6%	DLR, Köln	x		x	
VII	Al_2O_3 99.6%	Friedrichsfeld AG	x	x	x	x
VIII	Al_2O_3 99.6%	Friedrichsfeld AG	x	x	x	x
IX	Al_2O_3 97.3%	Feldmühle	x		x	x
X	Al_2O_3 + 5% ZrO_2	Desmarquest	x		x	
XI	Al_2O_3 + 10% ZrO_2	Desmarquest	x		x	
XII	AlN	[1]	x	x	x	
XIII	sapphire	Crystal Systems	x	x		

Table 1. Materials investigated. Material IX contains 2.7% SiO_2 ; materials I,X,XI,XII and XIII are first choice for HF-windows and also used for dielectric characterisation (R. Heidinger, KfK, IMF I).

In this table "SCG" means subcritical crack growth and "fatigue" is standing for cyclic fatigue. Two batches of sapphire were investigated:

1. HEMEX, taken from a gyrotron window of 3.5mm thickness,
2. HEMLITE, orientation (0001), surface: polished 80-50.

2.2 Spontaneous failure

2.2.1 Inert strength

The inert strength σ_c - responsible for spontaneous failure - can be described in most cases by a two-parametric Weibull distribution

$$F(\sigma_c) = 1 - \exp\left[-\left(\frac{\sigma_c}{\sigma_0}\right)^m\right] \quad (1)$$

where F denotes the cumulative density function and m , σ_0 are the Weibull parameters. For a data sample of N strengths, cumulative probabilities are calculated by ranking values in ascending order and evaluating one of the following relations

$$F_i = \frac{i-0.5}{N}, \quad F_i = \frac{i}{N+1}, \quad F_i = \frac{i-0.3}{N+0.4} \quad (2)$$

which are all widely used in the literature.

One possibility of determining m and σ_0 is to plot $\ln \ln 1/(1-F)$ against $\ln \sigma_c$. This should give a straight line of slope m and intercept $-m \ln \sigma_0$. A second possibility (more accurate but requiring more expenditure) is to apply the Maximum-Likelihood procedure proposed by Thoman et al. [2](see also [3]). In order to obtain an unbiased estimate m_{corr} for m , the bias factor $b(N)$ (N =number of tests) is introduced by Thoman et al. [2]. m_{corr} is given by

$$m_{corr} = m b(N) \quad (3)$$

where $b(N)$ can be approximated for $N > 5$ by [15]

$$b(N) \simeq \tanh^{1.87}\left(\frac{N-3.855}{0.678}\right)^{0.21375} \quad (4)$$

The inert strength data were determined under conditions of increasing bending load. Bending bars of 3.5x4.5x45mm were subjected to dynamic four-point bending tests in air with 20 mm inner span and 40 mm outer span. The tests were performed at a high loading rate of $\dot{\sigma} \simeq 200$ MPa/s to avoid subcritical crack propagation.

2.2.2 Fracture toughness

The fracture toughness K_{Ic} has been determined with edge-notched bending bars and in case of sapphire with the indentation method. In 4-point bending tests with the notched specimens the maximum outer fiber bending stress σ_{max} is determined and the fracture toughness is computed by

$$K_{Ic} = \sigma_{max} \sqrt{a} Y \quad (5)$$

where a is the notch depth and Y is the geometric function. For $0 < \alpha < 1$ Srawley and Gross [4] proposed

$$Y = \frac{1}{(1-\alpha)^{3/2}} \left[1.9887 - 1.326\alpha - \frac{\alpha(1-\alpha)}{(1+\alpha)^2} (3.49 - 0.68\alpha + 1.35\alpha^2) \right] \quad (6)$$

with $\alpha = a/W$ (W = specimen width).

The indentation fracture toughness can be determined by introducing a Vickers indenter in the specimen surface. In brittle materials cracks are generated. Their length $2c$ can be measured at the surface. If the indentation load is P and the diagonal of the indentation is $2a$ the fracture toughness results as [5]

$$K_{Ic} = 0.032 H \sqrt{a} (E/H)^{1/2} (c/a)^{-3/2}, \quad H = P/(2a^2) \quad (7)$$

E = Young's modulus, H = hardness.

2.3 Subcritical crack growth

2.3.1 Basic relations

The failure of ceramic materials is often caused by subcritical crack propagation. In the range of linear-elastic fracture mechanics crack growth is governed only by the stress intensity factor K_I

$$\frac{da}{dt} = v(K_I) \quad (8)$$

K_I describes the stresses near a crack tip and is generally written in the form

$$K_I = \sigma \sqrt{a} Y \quad (9)$$

where σ denotes the stress and a the depth of a crack in a structure, and Y is the geometric correction factor dependent on the shape of the crack and the component.

In many cases, the subcritical crack growth rates in ceramics can be described by a power law

$$v = AK_I^n = A^*(K_I/K_{Ic})^n \quad (10)$$

but unfortunately this simple relationship cannot be assumed to be valid a priori in all cases. This was the reason for developing procedures which allow to determine the complete v - K_I -curve, especially for very small crack growth rates relevant to lifetime predictions.

2.3.2 Lifetime method for the determination of v - K -curves

The lifetime procedures are based on the general lifetime relation for statically loaded ceramics [6]-[9]. By combining eqs.(9) and (10) the lifetime t_f follows as

$$t_f = \frac{2}{\sigma^2 Y^2} \int_{K_{Ii}}^{K_{Ic}} \frac{1}{v(K_I)} K_I dK_I \quad (11)$$

where K_{Ic} is the fracture toughness and K_{Ii} is the initial value of the stress intensity factor given by

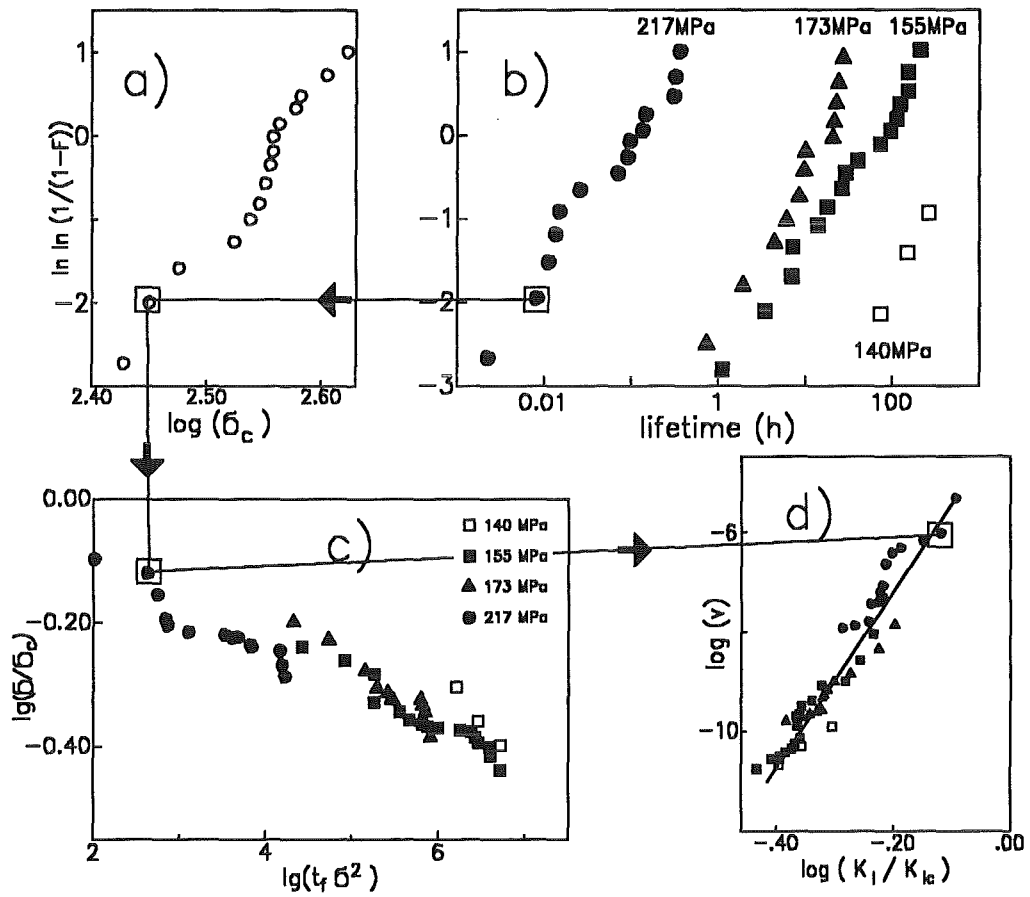


Figure 1. . Procedure of determining $v - K_I$ -curves for 99.6% Al_2O_3 . (normalised stress = σ/σ_c , normalised lifetime = $t_f \sigma^2$)

$$K_{II} = \sigma \sqrt{a_i} Y_i \quad (12)$$

Differentiating eq.(11) with respect to the initial stress intensity factor K_{II} one obtains [8]

$$v(K_{II}) = - \frac{2}{t_f \sigma^2} \left(\frac{K_{II}}{Y_i} \right)^2 \frac{d[\log(K_{II})]}{d[\log(t_f \sigma^2 Y_i^2)]} \quad (13)$$

This lifetime relation gives rise to a number of strategies aimed to obtain information on the sub-critical crack growth law. The most appropriate procedures will be listed in the following section and explained schematically.

As eq.(12) shows, the needed change in K_{II} can be generated either by introducing uniform small surface cracks and varying the stress applied or by use of a fixed stress and making use of the scatter of the natural cracks. The scatter of the initial crack size is related to the scatter of the inert strength σ_c by

$$K_{Ic} = \sigma_c \sqrt{a_i} Y_i \quad (14)$$

and with eq.(12) by

$$K_{II} = K_{Ic} \frac{\sigma}{\sigma_c} \quad (15)$$

Due to this relation and taking into account

$$d(\ln K_{II}/K_{Ic}) = d \ln K_{II} - d \ln K_{Ic} = d \ln K_{II} \quad (16)$$

one obtains a modified relation for evaluation

$$v(K_{II}) = - \frac{2K_{Ic}^2}{Y^2 \sigma_c^2 t_f} \frac{d(\ln \sigma / \sigma_c)}{d(\ln t_f \sigma^2)} \quad (17)$$

The procedure of evaluation $v(K_I)$ is relatively simple [8]. Figure 2 illustrates the procedure. In a first series of tests N samples are tested in dynamic tests at high stress rates in an inert environment to give the distribution of the inert strength σ_c (fig.1a). The N values of strength are arranged in an increasing order. In a second series, also involving N specimens, the lifetimes t_f were measured. The results are also arranged in increasing order (fig.1b). The v -th value of lifetime $t_{f,v}$ is associated with the v -th value of inert strength $\sigma_{c,v}$. The auxiliary diagram (fig.1c) provides the derivative needed in eq.(13)

To be able to apply the statistical method it has to be ensured that the same crack population is responsible for strength as for lifetimes. For application of the statistical procedure it is very important that lifetimes as well as strength measurements are performed using the same loading configuration. This is indispensable since the scatters in lifetime and strength must not be influenced by the use of different testing devices.

2.4 Cyclic fatigue

2.4.1 Basic relations

The results of tests under cyclic loading can be presented as σ - N -curves, with the stress amplitude σ_a or the maximum stress σ_{\max} plotted versus the number of cycles until failure. It is also possible to derive from such tests the da/dN - ΔK -relation of the material.

The crack growth in one load cycle da/dN is a function of the range of the stress intensity factor

$$\frac{da}{dN} = f(\Delta K) , \quad (18)$$

where ΔK is dependent on the stress range $\Delta\sigma$ and the crack depth a by

$$\Delta K = \Delta\sigma\sqrt{a} Y \quad (19)$$

Instead of the stress range, the stress amplitude $\sigma_a = \Delta\sigma/2$ or the maximum stress can be used. Then, with $R = \sigma_{\min}/\sigma_{\max}$,

$$\Delta K = 2\sigma_a\sqrt{a} Y \quad (20)$$

$$\Delta K = \sigma_{\max}(1 - R)\sqrt{a} Y \quad (21)$$

In many cases also the cyclic fatigue crack growth data may be represented by a power law relation

$$\frac{da}{dN} = A(\Delta K)^n \quad (22)$$

or

$$\frac{da}{dN} = A^* \left(\frac{\Delta K}{K_{Ic}} \right)^n \quad (23)$$

Then, the number of cycles until failure is

$$N_f = \frac{B\sigma_c^{n-2}}{(\Delta\sigma)^n} = \frac{B\sigma_c^{n-2}}{\sigma_{\max}^n(1-R)^n} = \frac{C}{\sigma_{\max}^n(1-R)^n} \quad (24)$$

with

$$B = \frac{2}{A(n-2)Y^2K_{Ic}^{n-2}} \quad \text{and} \quad C = B\sigma_c^{n-2} \quad (25)$$

In a plot of $\lg \Delta\sigma$ or $\lg \sigma_{\max}$ versus $\lg N_f$ a straight line with a slope of $-1/n$ is expected.

2.4.2 Statistical procedure

A statistical procedure to determine the da/dN - ΔK -relation is developed in [17]. It is analogous to the method developed by the authors for static tests [8]. It does not assume a power-law relation between da/dN and ΔK . The evaluation procedure uses the general relation

$$N_f = \int_{a_i}^{a_c} \frac{da}{\frac{da}{dN}(\Delta K)} = \frac{2}{(\Delta\sigma Y)^2} \int_{\Delta K_i}^{\Delta K_c} \frac{\Delta K d(\Delta K)}{\frac{da}{dN}(\Delta K)} \quad (26)$$

with

$$\Delta K_i = \Delta\sigma Y \sqrt{a_i} \quad (27)$$

$$\Delta K_c = \Delta\sigma Y \sqrt{a_c} = \Delta\sigma_c Y \sqrt{a_i} \quad (28)$$

$$\text{and } \Delta\sigma_c = \sigma_c(1 - R) \quad (29)$$

This first-kind Volterra integral equation can be solved by differentiation and one obtains

$$\frac{d(N_f \Delta\sigma^2 Y^2)}{d(\Delta K_i)} = -2 \frac{\Delta K_i}{\frac{da}{dN}(\Delta K_i)} \quad (30)$$

Assuming that the same flaws are responsible for fatigue failure and for strength, the initial crack size can be replaced by the inert fracture strength and ΔK_i by

$$\Delta K_i = \frac{\Delta\sigma}{\sigma_c} K_{Ic} \quad (31)$$

Equation (30) then leads to the crack growth rate da/dN at the beginning of the cyclic test ($\Delta K = \Delta K_i$):

$$\frac{da}{dN}(\Delta K_i) = - \frac{2K_{Ic}^2}{N_f \sigma_c^2 Y^2} \frac{d \log(\Delta\sigma/\sigma_c)}{d \log(N_f \Delta\sigma^2)} \quad (32)$$

If the initial crack size can be measured, eq.(30) can be replaced by

$$\frac{da}{dN}(\Delta K_i) = - \frac{2a_i}{N_f} \frac{d \log(\Delta\sigma \sqrt{a_i} Y)}{d \log(N_f \Delta\sigma^2 Y_i^2)} \quad (33)$$

The evaluation of eq.(32) requires the relation between $\Delta\sigma/\sigma_c$ and $N_f \Delta\sigma^2$. The basic idea is to use the natural scatter of the strength and the lifetime and to correlate the corresponding values for the same failure probability.

If for the strength test and the lifetime test the same specimen size is used, then a number of N specimens are used for strength and lifetime measurements. The results are ranked and corresponding values (j th strength and j th lifetime) are used in a $\log(\Delta\sigma/\sigma_{cj})$ versus $\log(N_{fj} \Delta\sigma^2)$ plot. From this plot the slope is determined and da/dN calculated for the corresponding N_{fj} , σ_{cj} according to eq.(32). The corresponding ΔK_{ij} is given by

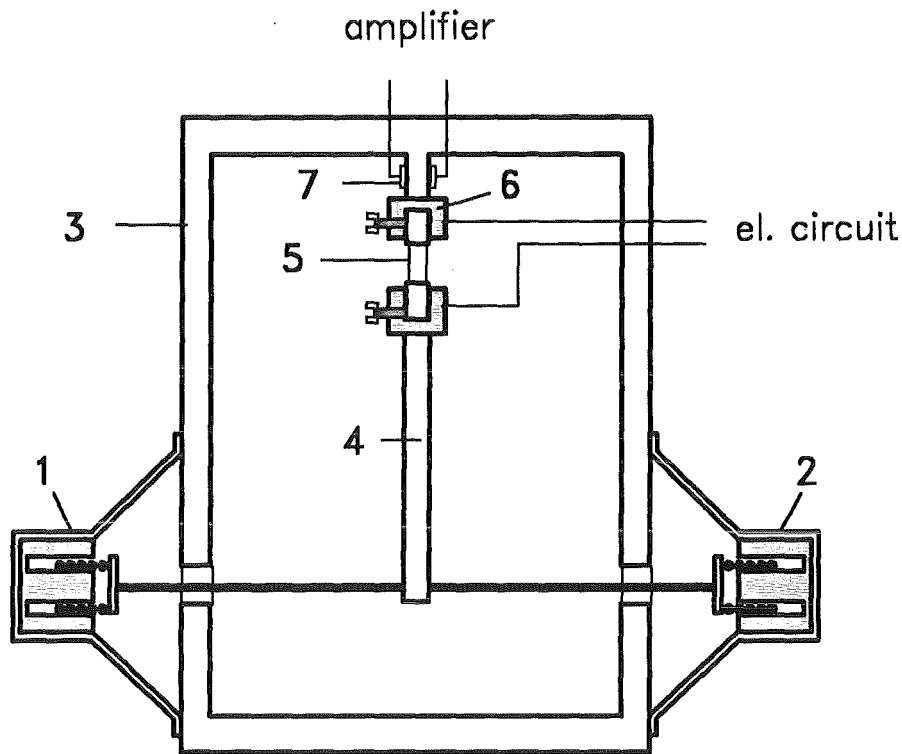


Figure 2. . Cyclic-fatigue arrangement driven by loudspeakers.

$$\Delta K_{ij} = \frac{\Delta \sigma}{\sigma_{cj}} K_{Ic} \quad (34)$$

2.4.3 Testing device

Cyclic fatigue tests were carried out in alternating bending tests loaded with loudspeakers in a cantilever arrangement. A simple testing device ([10]) is shown in fig.2. The cyclic load is generated by the magnet system of loudspeakers (1,2) - fixed at the frame (3) - and transferred to the specimen by a cantilever (4). The specimen (5) is clamped in the specimen holders (6) and the bending moment is measured by strain gauges (7) provided on the fixing bracket as well as directly on special specimens used for calibration. The specimen itself (5) is fixed at its ends in **brass tubes** (8) by an epoxy resin (10) (see fig.3). Due to the low Young's modulus of the epoxy resin compared with the Young's modulus of the ceramic specimen, the load can be applied without any notch effect. The second type of specimen fixing is recommended for materials with a relatively low Young's modulus. At the moment of failure, a silver strip (9) on the specimen is interrupted, the loudspeaker stops working and a time counter is stopped.

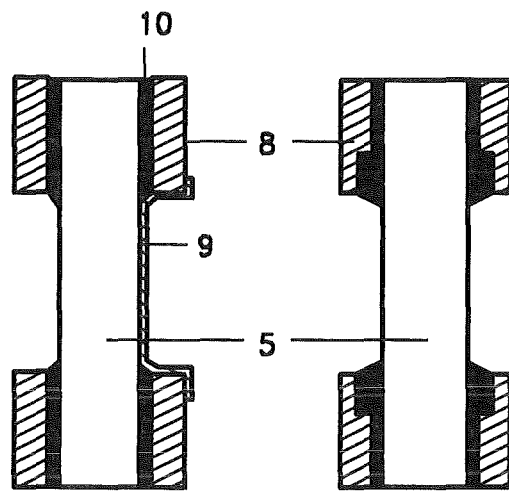


Figure 3. . Specimens for fatigue tests.

3. Failure prediction

The stresses in the ceramic window may cause spontaneous failure because they are higher than the strength of the component, and also delayed failure due to subcritical extension of small flaws or cracks leading to failure after some time of operation.

3.1 Spontaneous failure

The strength σ_c usually measured in a bending test may be described by a Weibull distribution with the cumulative density function given in eq.(1)

$$F = 1 - \exp[-(\sigma_c/\sigma_0)^m]$$

The parameter σ_0 is dependent on the size and stress distribution of the entire component. Equation (1) has to be modified to take into account the size effect. The stress distribution is written as

$$\sigma = \sigma^* \cdot g(x, y, z) \quad (35)$$

where σ^* is a reference stress in the component - e.g. the maximum stress - and g is a function dependent only on the geometry. For surface flaws eq.(1) has to be replaced by

$$F = 1 - \exp\left[-\frac{1}{S_0} (\sigma^*/\sigma_s)^m \int g^m dS\right] = 1 - \exp\left[-\frac{S_{eff}}{S_0} (\sigma^*/\sigma_s)^m\right] \quad (36)$$

where S_0 is the unit area and σ_s is a size-independent parameter. S_{eff} is an effective area given by

$$S_{eff} = \int g^m dS \quad (37)$$

If the fracture strength is determined in a bending test, σ_c is the outer fibre stress at failure and thus $\sigma_c = \sigma^*$. The failure stress of a component for a given failure probability F is obtained from eq.(36) as

$$\sigma^* = \sigma_s \left(\frac{S_0}{S_{eff,c}}\right)^{1/m} \left[\ln \frac{1}{1-F}\right]^{1/m} = \sigma_0 (S_{eff,sp}/S_{eff,c})^{1/m} \left[\ln \frac{1}{1-F}\right]^{1/m} \quad (38)$$

where σ_0 is the Weibull parameter measured in the bending test, and $S_{eff,sp}$ and $S_{eff,c}$ are the effective areas of the specimens and the component, respectively.

3.2 Delayed failure

It can be shown that the time to failure can also be described by a Weibull-distribution

$$F = 1 - \exp[-(t_f/t_0)^{m^*}] \quad (39)$$

with

$$m^* = \frac{m}{n-2}, \quad t_0 = B\sigma_0^{n-2}\sigma^{-n} \quad (40)$$

Equation (39) is correct if the effective specimen surfaces for determination of the strength are identical to the effective area of the component. Otherwise,

$$t_0 = B\sigma_0^{n-2}\sigma^{*-n} [S_{eff,sp}/S_{eff,c}]^{(n-2)/m} \quad (41)$$

For a given failure probability the time to failure is

$$t_f = \left[\ln \frac{1}{1-F} \right]^{(n-2)/m} B\sigma_0^{n-2}\sigma^{*-n} [S_{eff,sp}/S_{eff,c}]^{(n-2)/m} \quad (42)$$

The failure behaviour of the HF-window can be described by eqs.(38) and (42). This is outlined in [13] and [3].

The lifetime of the window is obtained by integration of the crack-growth relation between the initial crack size a_i and the critical crack size a_c , leading to

$$t_f = \frac{2}{AY^n\sigma^n(n-2)} [a_i^{(2-n)/2} - a_c^{(2-n)/2}] \quad (43)$$

Because of the high n-values observed, the second term in the brackets can be neglected. The initial crack size a_i can be determined indirectly by measurement of the strength σ_c in a rapid loading test where subcritical crack extension can be avoided and by applying the relation

$$K_{Ic} = \sigma_c \sqrt{a_i} Y \quad (44)$$

Then, the time to failure is given by

$$t_f = B\sigma_c^{n-2}\sigma^{-n} \quad (45)$$

with

$$B = \frac{2}{(n-2)AY^2K_{Ic}^{n-2}} = \frac{2}{(n-2)A^*Y^2} K_{Ic}^2 \quad (46)$$

Equation (45) relates the time to failure to the fracture strength. The fracture strength and the time to failure show a considerable amount of scatter.

4. Results

The results are represented in the following way:

- **Strength**
 - plotted as Weibull-diagram of strength,
 - described by the Weibull-parameters σ_0 and m .
- **Fracture toughness**
 - listed in Table 3.
- **Subcritical crack growth**
 - represented by the v-K-curves of subcritical crack growth,
 - described by the parameters A or A^* and n of the power-law relation (10).
- **Crack growth under cyclic load**
 - plotted as Wöhler-curves,
 - plotted as da/dN - ΔK -curves,
 - described by the parameters A or A^* and n of the power-law relation (23).

4.1 Parameters and references to curves in the Appendix

1. Material I
 - a. Strength (see fig.4).
 - b. v-K-curve, measured in fluorocarbon FC43 at 50°C (see fig.5).
 - c. $\log_{10}A^* = -4.5$ (A^* in m/s), $n = 45$.
2. Material II
 - a. Strength (see fig.6).
 - b. v-K-curve, measured in concentrated salt solution at $\approx 70^\circ\text{C}$ (see fig.7).
 - c. $\log_{10}A^* = -3.5$ (A^* in m/s), $n = 20$.
3. Material III

- a. Strength (see fig.8).
 - b. v-K-curve, measured in concentrated salt solution at $\approx 70^\circ\text{C}$ (see fig.9).
 - c. $\log_{10}A^* = -2.6$ (A^* in m/s), $n = 48$.
4. Material IV
- a. Strength (see fig.10).
 - b. v-K-curve, measured in concentrated salt solution at $\approx 70^\circ\text{C}$ (see fig.11).
 - c. $\log_{10}A^* = 5$ (A^* in m/s), $n = 73.5$.
5. Material V
- a. Strength (see fig.12).
 - b. v-K-curve, measured in fluorocarbon FC43 at 50°C . (see fig.13).
 - c. $\log_{10}A^* = -1$ (A^* in m/s), $n = 33$.
 - d. v-K-curve, measured in water of 20°C (see fig.14).
 - e. $\log_{10}A^* = 2$ (A^* in m/s), $n = 51$.
 - f. Influence of the environment on the v-K-data (see fig.15).
6. Material VI
- a. Strength (see fig.16).
 - b. v-K-curve (see fig.17).
 - c. $\log_{10}A^* = -2.5$ (A^* in m/s), $n = 48$.
7. Materials VII and VIII
- a. Strength (see fig.18).
 - b. v-K-curve for material VII (air, 20°C) for natural cracks and artificial cracks introduced by Knoop-indentation tests (see fig.19).
 - c. $\log_{10}A^* = -3.5$ (A^* in m/s), $n = 39$.
 - d. Wöhler-curves for static and cyclic tests on specimens with natural flaw population (material VII) (see fig.20).
 - e. Wöhler-curves for static and cyclic tests carried out with Knoop-damaged specimens (material VII) (see fig.21).
 - f. $da/dN-\Delta K$ -curves resulting from the cyclic tests of figs.20 and 21 (see fig.22).
 - g. $\log_{10}A^* = -5.3$ (A^* in m/cycle), $n = 29$.
 - h. Lifetime in static tests (air, 20°C) for material VIII; (see fig.23).
 - i. Influence of the R-ratio on lifetimes (Knoop-damaged specimens, material VIII); (see fig.24).
 - j. Influence of the frequency on lifetimes (specimens with natural flaws, material VIII); (see fig.25).

- k. Influence of the frequency on the $da/dN-\Delta K$ -curve (natural flaws, material VIII); (see fig.26).
 - l. Influence of the R-ratio on the $da/dN-\Delta K$ -curve (Knoop-damaged specimens, material VIII); (see fig.27).
8. Material IX
- a. Strength (see fig.28).
 - b. v-K-curve in water at 20°C (see fig.29).
 - c. $\log_{10}A^* = -5.5$ (A^* in m/s), $n = 32$.
 - d. $da/dN-\Delta K$ -curves at 20°C in air (see fig.30).
 - e. $\log_{10}A^* = -4.5$ (A^* in m/cycle), $n = 26$.
9. Material X
- a. Strength (see fig.31).
 - b. v-K-curve, measured in fluorocarbon FC43 at 50°C (see fig.32).
 - c. $\log_{10}A^* = -5.2$ (A^* in m/s), $n = 32$.
10. Material XI
- a. Strength (see fig.33).
 - b. v-K-curve, measured in fluorocarbon FC43 at 50°C (see fig.34).
 - c. $\log_{10}A^* = -7.4$ (A^* in m/s), $n = 14$.
11. Material XII
- a. Strength (see fig.35).
 - b. v-K-curve, measured in fluorocarbon FC43 at 50°C (see fig.36).
 - c. $\log_{10}A^* = -3$ (A^* in m/s), $n = 135$.
12. Material XIII
- a. Strength of bending bars cut out of a sapphire disc (see fig.37).
 - b. Testing device for ring-on-ring tests (see fig.38).
 - c. Strength of sapphire discs measured in ring-on-ring tests; one series of discs were additionally heat-treated (see fig.38).
13. Comparison of first-choice materials
- a. Bending strength.
 - b. v-K-curves.

Number	Material	Ref.	σ_0 (MPa)	m	n_{static}	n_{cyclic}
I	Al_2O_3 99.99%		410	6	45	
II	Al_2O_3 >99.9%	[9] [13]	369	10.4	20	
III	Al_2O_3 >99.9%	[11] [13]	434	9.7	48	
IV	Al_2O_3 >99.9%	[12] [13]	383	10	73.5	
V	Al_2O_3 99.7%	[1] [16]	335/420	7.4/10	51/33	
VI	Al_2O_3 99.6%	[14]	420	14	48	
VII	Al_2O_3 99.6%	[17]			39	23-29
VIII	Al_2O_3 99.6%				≈ 90	28-35
IX	Al_2O_3 97.3%	[19] [18]	365	16.5	32	26
X	$Al_2O_3 + 5\%ZrO_2$		560	8	32	
XI	$Al_2O_3 + 10\%ZrO_2$		577	8.5	14	
XII	AlN	[1] [16]	310	15.3	135	
XIII	sapphire		975	9		

Table 2. Comparison of the investigated materials. For material V the first value of n_{static} is obtained for water, the second one for fluorocarbon; the strength data of sapphire type HEMEX were excluded.

For several materials also the fracture toughness K_{Ic} was determined. The measurements were carried out with edge-notched specimens containing a saw cut of $50\mu m$ width. In case of material XIII the indentation method [5] was applied. Vickers indentations were introduced in specimens of the HEMLITE quality with 49N indentation load.

material	K_{Ic} (MPa \sqrt{m})
II	4.0
III	3.9
IV	3.8
V	4.5
VII	3.3
VIII	3.3
XII	3.2
XIII	1.97

Table 3. Fracture toughness K_{Ic} . Edge-notched bending bars; material XIII: indentation method, 49N indentation load.

From the mean value of $a = 40.75\mu m$ the hardness was determined as

$$H = \frac{P}{2a^2} = 14.8 \text{ GPa}$$

The measured c -values were: $c = 164\mu m$ with a standard deviation of $16\mu m$. Using the Youngs modulus for dense Al_2O_3 , $E = 410 \text{ GPa}$ [3], it results from eq.(7): $K_{Ic} = 1.97 \text{ MPa}\sqrt{m}$ with a standard deviation of $0.3 \text{ MPa}\sqrt{m}$.

5. References

- [1] T. Fett, D. Munz, in: Proceedings of the 15. SOFT (Utrecht, 1988) p.899.
- [2] D.R. Thoman, L.J. Bain, C.E. Antle, Inferences on the parameters of the Weibull-distribution, *Technometrics* **11**(1969)445-460.
- [3] D. Munz, T. Fett, *Mechanisches Verhalten keramischer Werkstoffe*, Springer Verlag 1989.
- [4] J.E. Srawley, B. Gross, Side-cracked plates subject to combined direct and bending forces, ASTM STP 601, Philadelphia, 1976.
- [5] G.R. Anstis, P. Chantikul, B.R. Lawn, D.B. Marshall, A critical evaluation of indentation techniques for measuring fracture toughness: I, Direct crack measurements, *J. Amer. Ceram. Soc.* **64**(1981),533-538.
- [6] A.G. Evans, S.M. Wiederhorn, Proof testing of ceramic materials - an analytical basis for failure prediction, *Int. J. Fract.* **10**(1974),379-392.
- [7] J.E. Ritter, Engineering design and fatigue failure of brittle materials, *Fracture Mechanics of Ceramics VI*, Plenum Press, 1978, 667-686.
- [8] T. Fett, D. Munz, Determination of v - K_I -curves by a modified evaluation of lifetime measurements in static bending tests, *Commun. of the Amer. Ceram Soc.* **68**,(1985) C213-C215.
- [9] T. Fett, K. Keller, D. Munz, Determination of crack growth parameters of alumina in 4-point bending tests, NAGRA Technical Report 85-51, Sept. 1985, Baden, Switzerland.
- [10] T. Fett, G. Thun, German Design Patent G 9107645.5.
- [11] T. Fett, W. Hartlieb, K. Keller, D. Munz, "Subcritical crack growth in high-grade alumina for container applications", Technical Report 87-09, NAGRA, Baden, Switzerland, Sept. 1987.
- [12] T.Fett, W. Hartlieb, K. Keller, D. Munz, W. Rieger, Subcritical crack growth in hot-isostatically postcompacted high grade alumina, Technical Report 89-13, NAGRA, Baden, Switzerland, April 1989.
- [13] T.Fett, W. Hartlieb, K. Keller, B. Knecht, D. Munz, W. Rieger, Subcritical crack growth in high-grade alumina, *Journal of Nuclear Materials* **184**(1991)39-46.
- [14] T. Fett, Lebensdauervorhersage an keramischen Werkstoffen mit den Methoden der Bruchmechanik bei elastischem und viskoelastischem Materialverhalten, doctoral thesis, Universität Karlsruhe 1983.
- [15] T. Fett, D. Munz, G. Thun, Influence of frequency on cyclic fatigue of coarse-grained Al_2O_3 , *J. Mater. Sci. Letters* **12**(1993)220-222.
- [16] T. Fett, D. Munz, Lifetime evaluation of ceramic windows in microwave heating tubes for fusion reactors, *J. Nucl. Mater.* **171**(1990),172-179.
- [17] T. Fett, G. Martin, D. Munz, G. Thun, *J. Mater. Sci.* **26**,3320(1991).
- [18] T. Fett, M. Mißbach, D. Munz, Failure behaviour of Al_2O_3 with glassy phase at high temperatures, *J. Europ. Ceram. Soc.* **13**(1994),197-209.
- [19] T. Fett, D. Munz, Static and cyclic fatigue of ceramic materials, Proc. of the 7th CIMTEC, 24/30 June 1990.

6. Appendix

Diagrams of strength and fatigue data

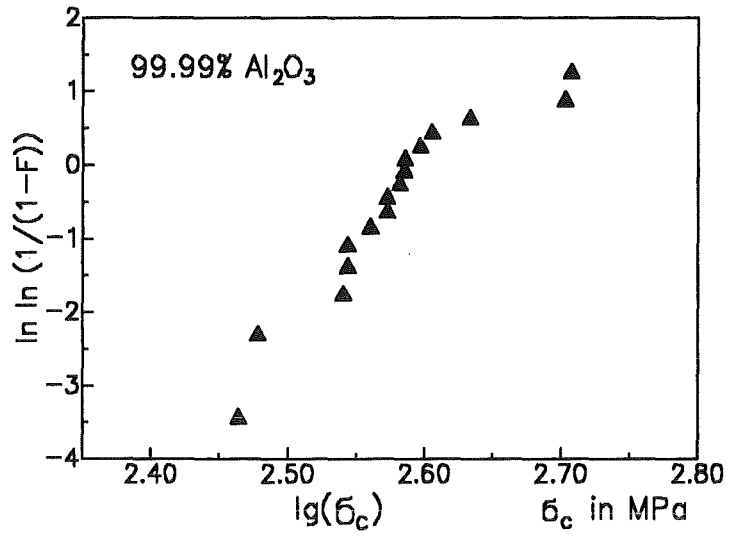


Figure 4. . Weibull-representation of bending strength (material I).

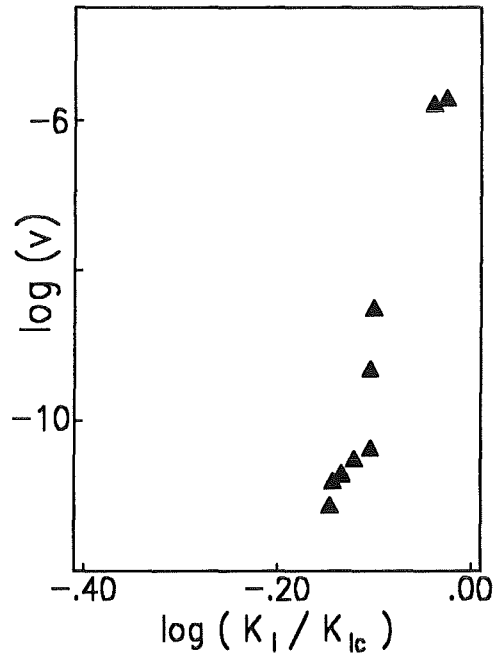


Figure 5. . v-K-curve for material I in fluorocarbon FC43 (50°C).

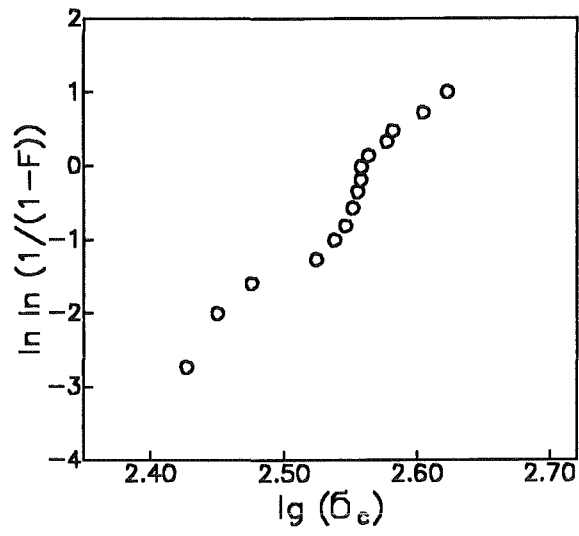


Figure 6. . Weibull-representation of bending strength (material II).

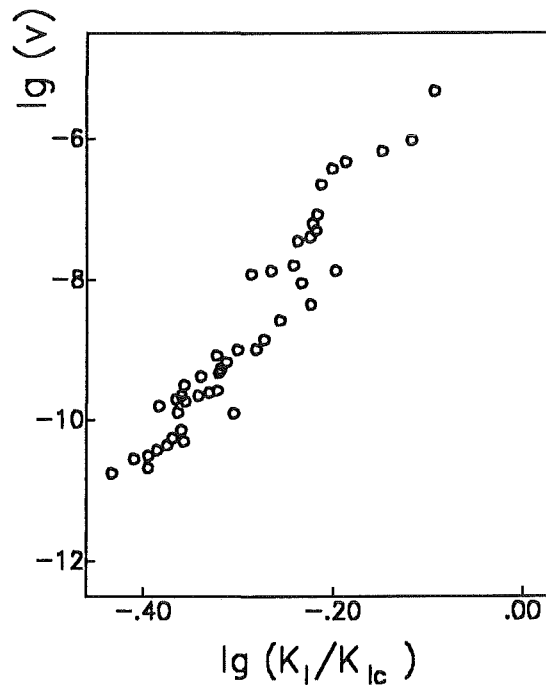


Figure 7. . v-K-curve for material II (salt-solution, 70°C).

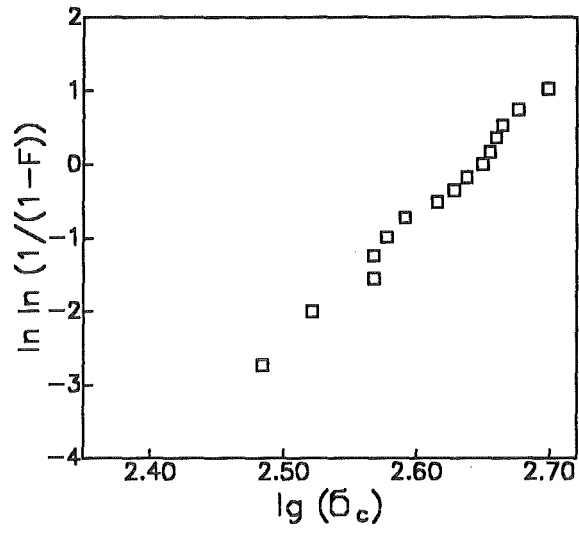


Figure 8. . Weibull-representation of bending strength (material III).

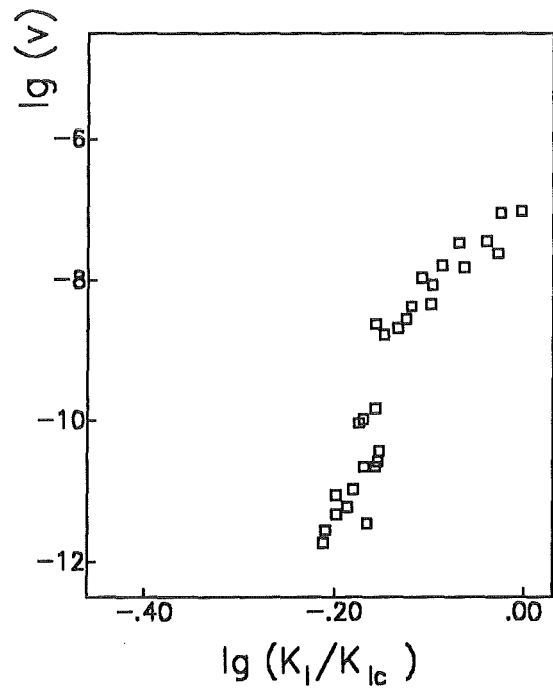


Figure 9. . v-K-curve for material III (salt-solution, 70°C).

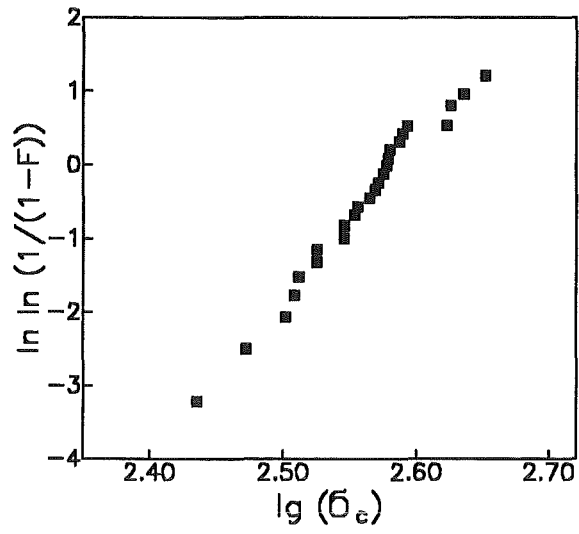


Figure 10. . Weibull-representation of bending strength (material IV).

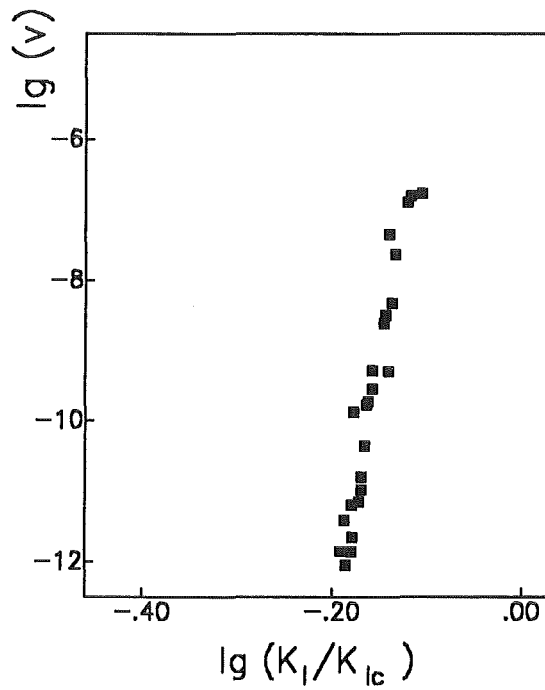


Figure 11. . v-K-curve for material IV (salt-solution, 70°C).

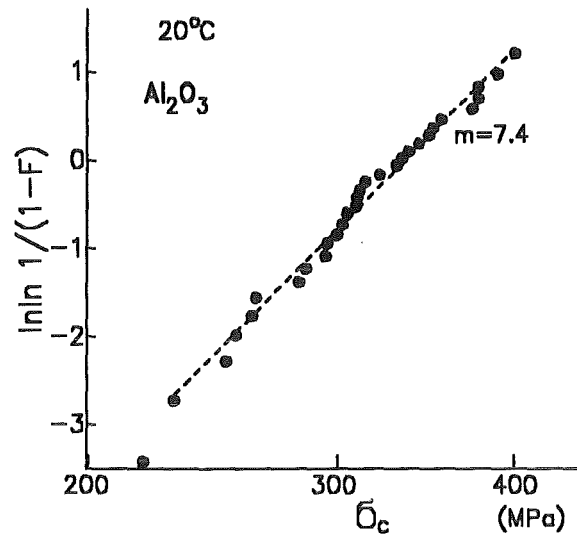


Figure 12. . Weibull-representation of bending strength (material V).

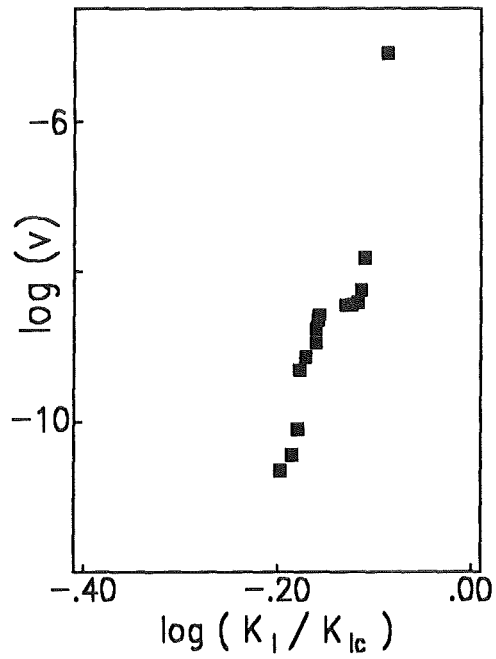


Figure 13. . v-K-curve for material V (measured in fluoro-carbon FC34, 50°C).

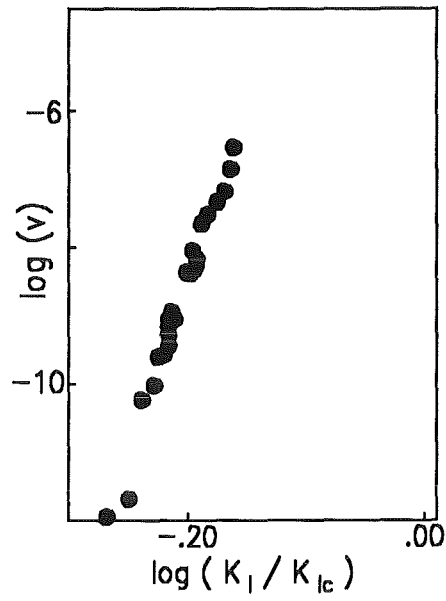


Figure 14. . v-K-curve for material V (measured in water at 20°C).

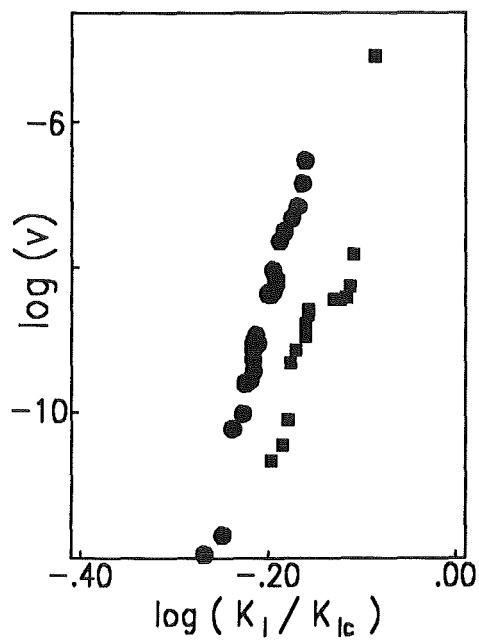


Figure 15. . Influence of the environment on the crack-growth rates (fig.13 compared with fig.14).

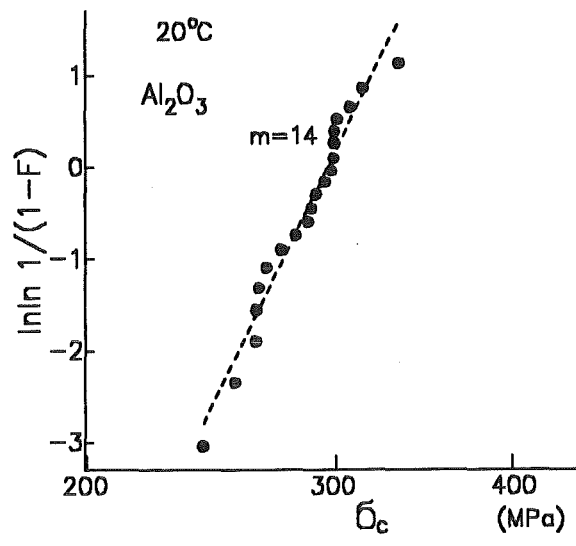


Figure 16. . Weibull-representation of bending strength (material VI).

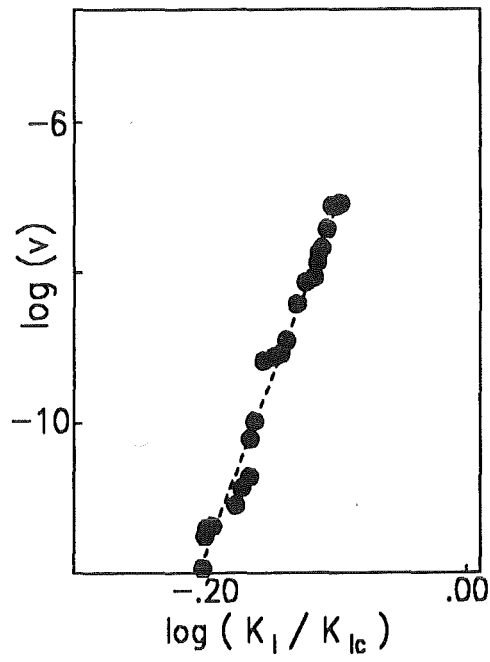


Figure 17. . v-K-curve for material VI (measured in water at 20°C).

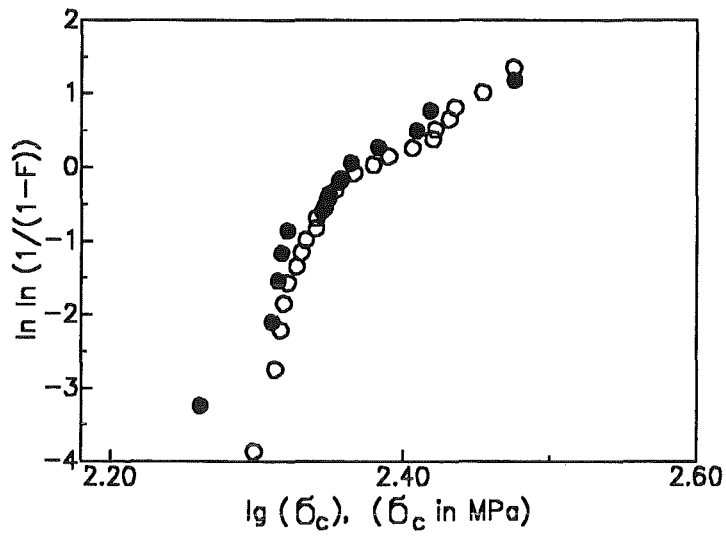


Figure 18. . Weibull-representation of bending strength (material VII: open circles), (material VIII: solid circles).

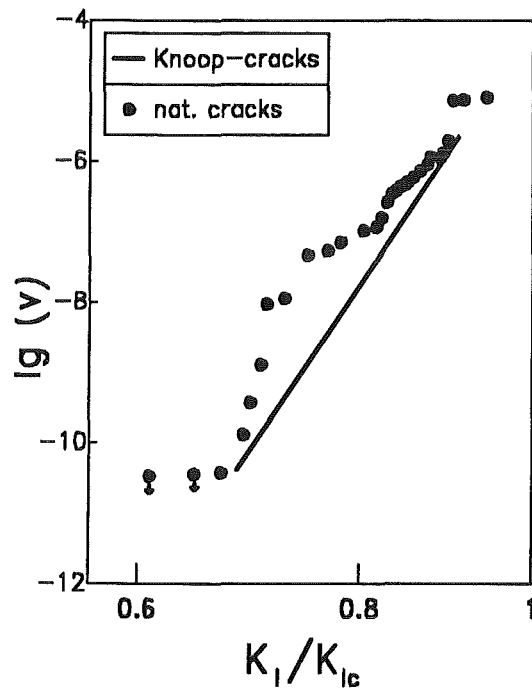


Figure 19. . v-K-curve for material VII (in air) for natural cracks and artificial cracks introduced by Knoop-indentation tests

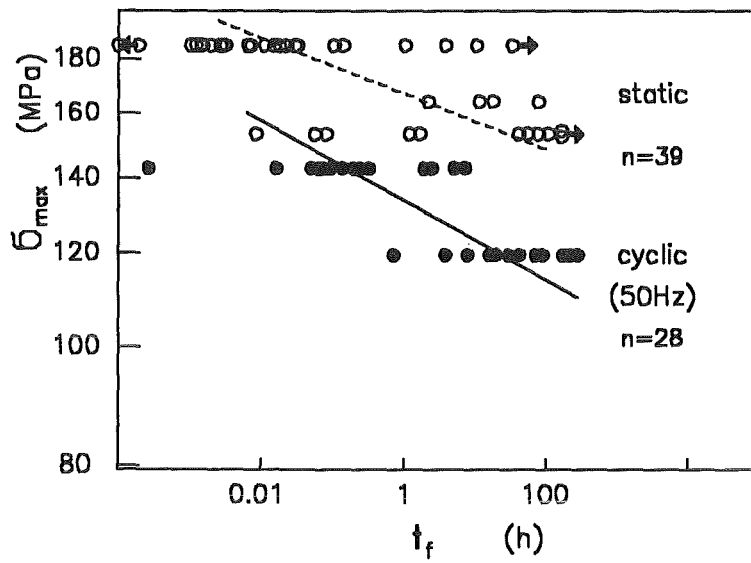


Figure 20. . Wöhler curves for static and cyclic tests on specimens with natural flaw population (material VII).

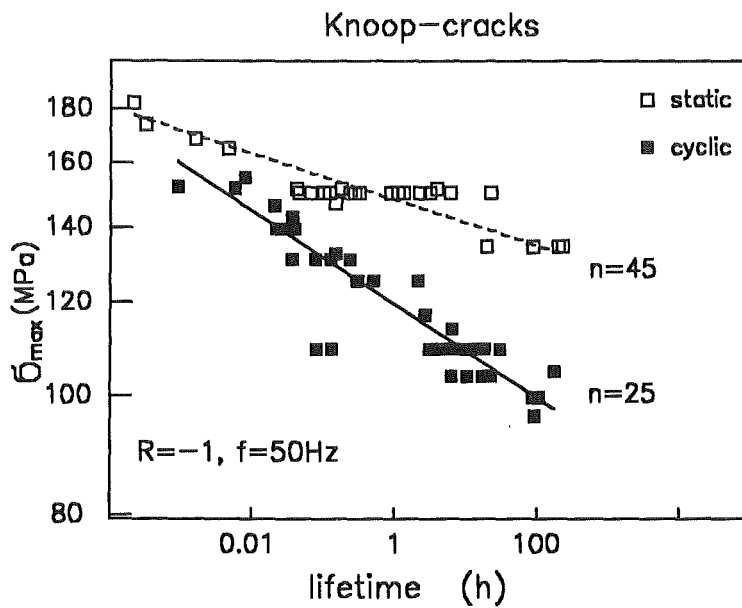


Figure 21. . Wöhler curves for static and cyclic tests on specimens with Knoop-cracks (material VII).

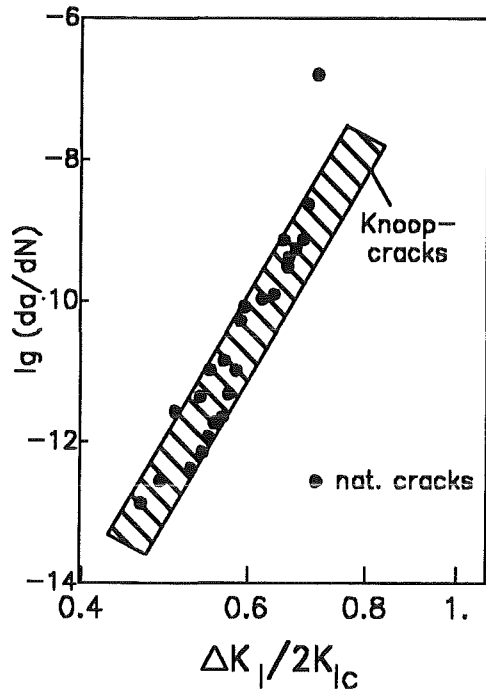


Figure 22. . da/dN-ΔK-curves resulting from the cyclic tests of figs.20 and 21 (in air, 20°C).

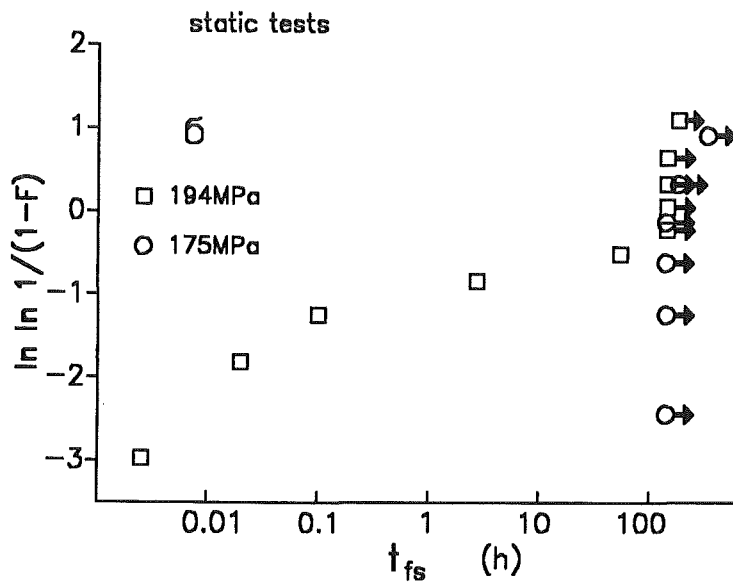


Figure 23. . Static lifetime tests in air (material VIII).

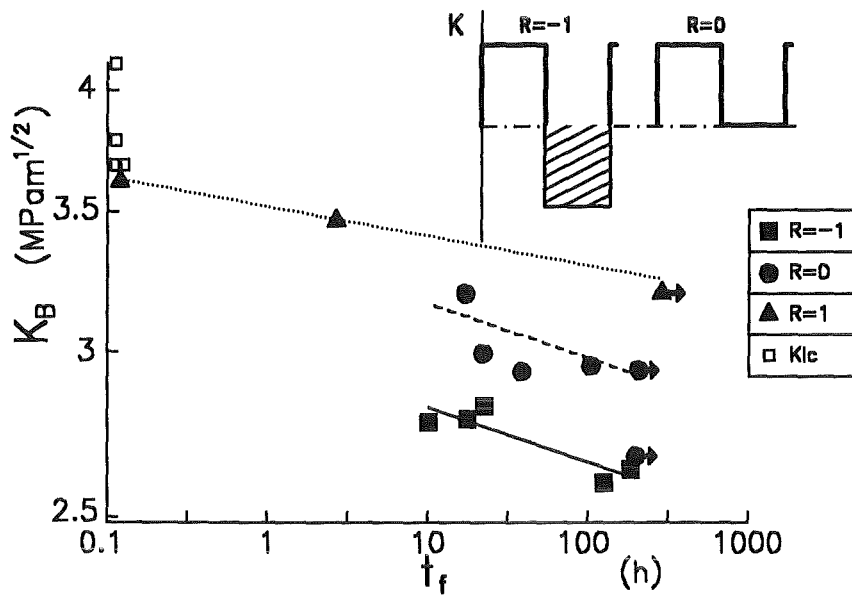


Figure 24. . Influence of the R-ratio on lifetimes (Knoop-damaged specimens, material VIII).

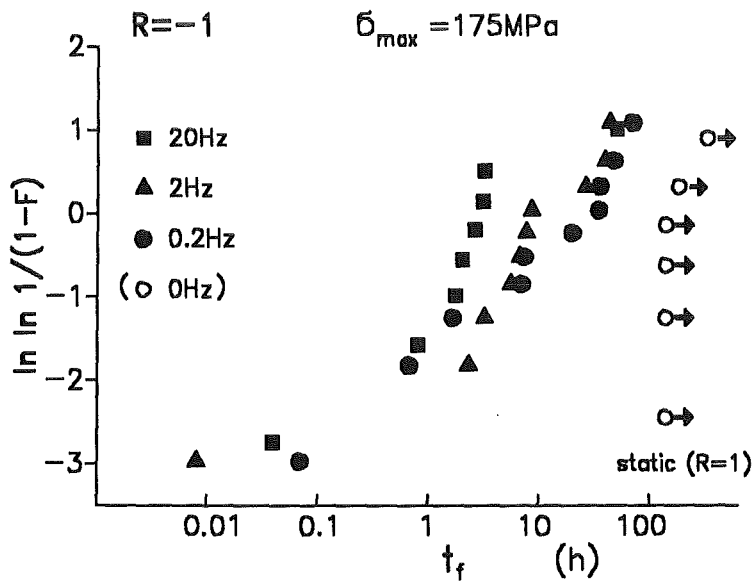


Figure 25. . Influence of the frequency on lifetimes (specimens with natural flaw population, material VIII).

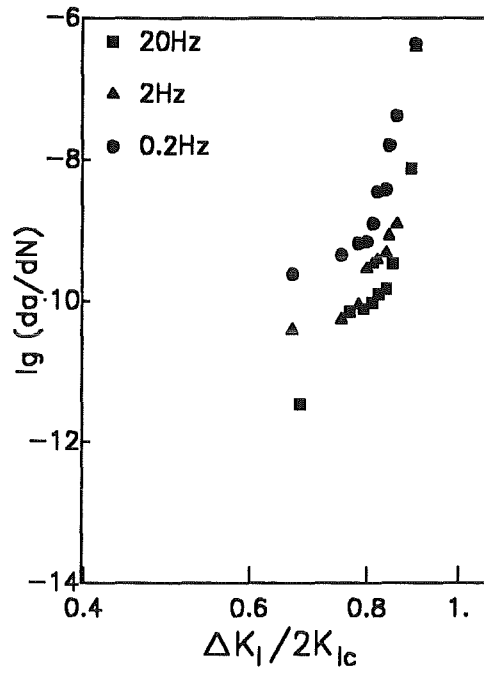


Figure 26. . Influence of the frequency on the da/dN- ΔK -curve (material VIII).

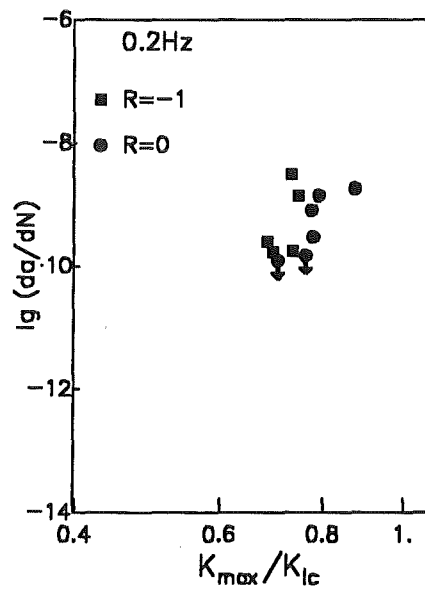


Figure 27. . Influence of the R-ratio on the da/dN- ΔK -curve (Knoop-damaged specimens, material VIII).

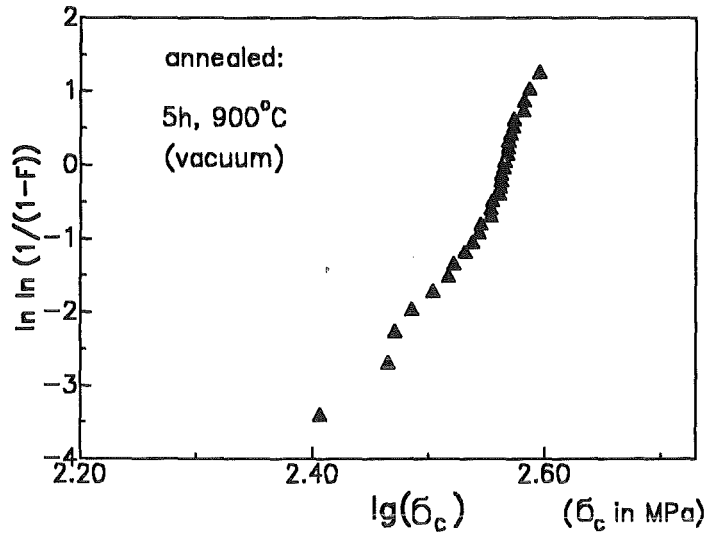


Figure 28. . Weibull-representation of bending strength (material IX).

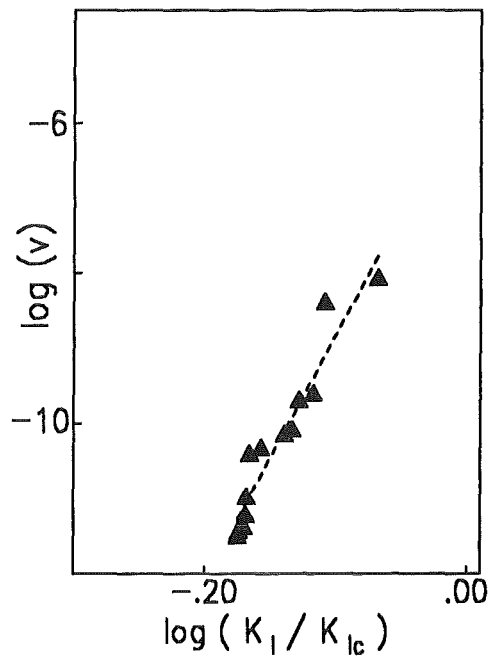


Figure 29. . v-K-curve for material IX (in water at room temperature).

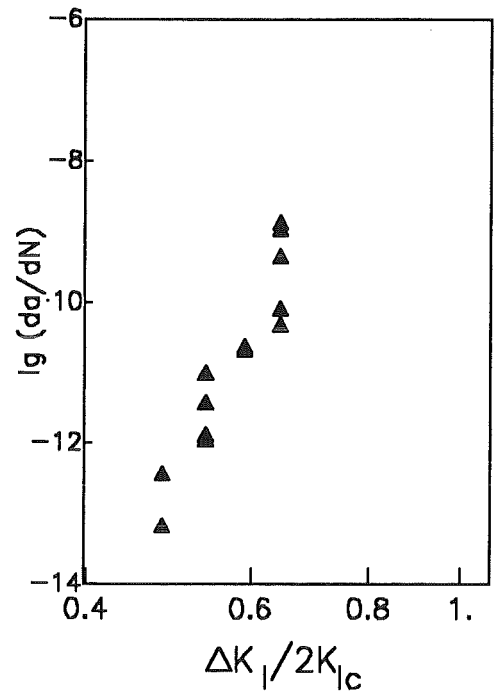


Figure 30. . da/dN-ΔK-curve for material IX (in air, 20°C).

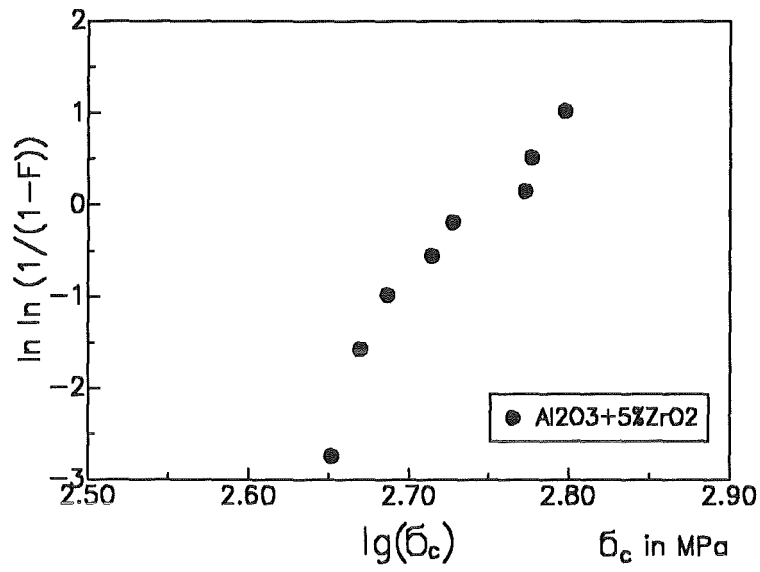


Figure 31. . Weibull-representation of bending strength (material X).

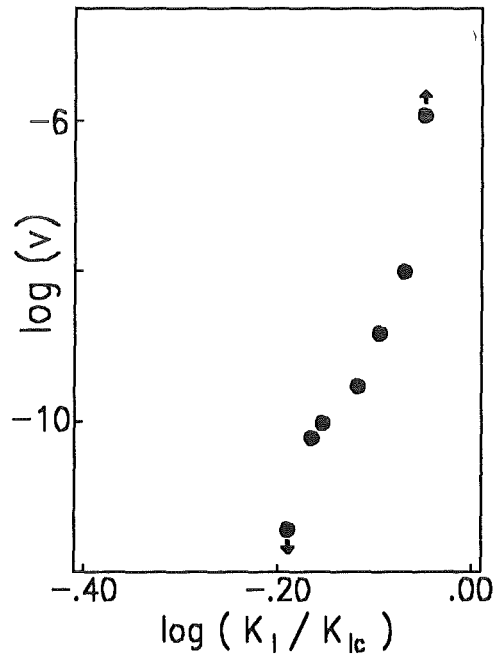


Figure 32. . v-K-curve for material X, measured in FC43 at 50°C.

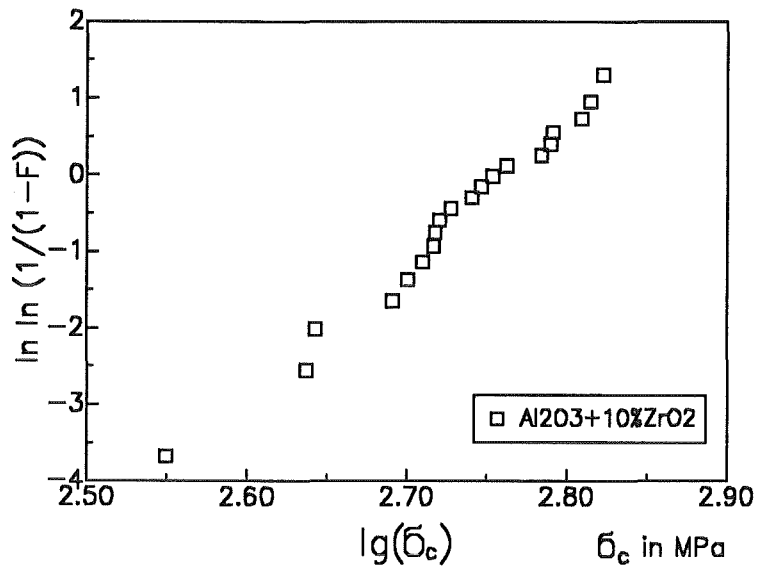


Figure 33. . Weibull-representation of bending strength (material XI).

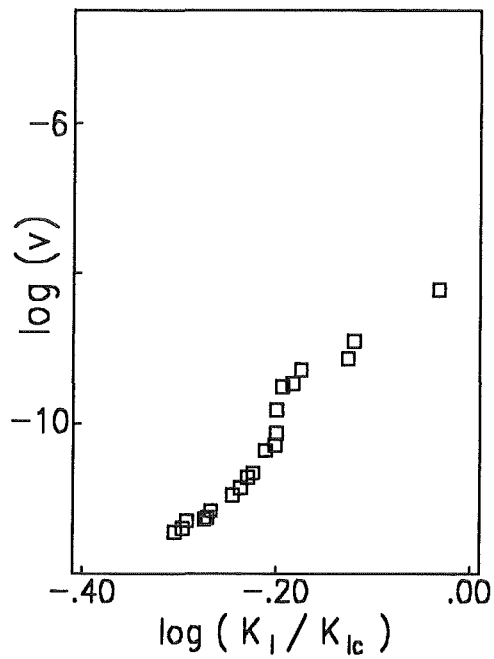


Figure 34. . v-K-curve for material XI, measured in FC43 at 50°C.

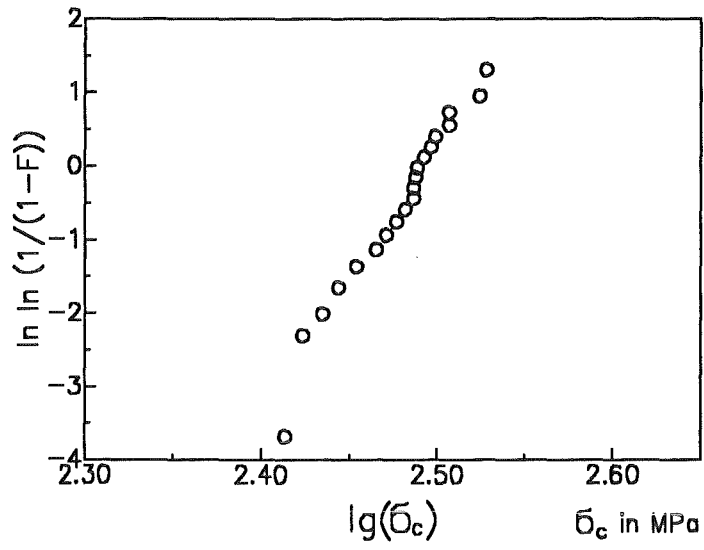


Figure 35. . Weibull-representation of bending strength (material XII).

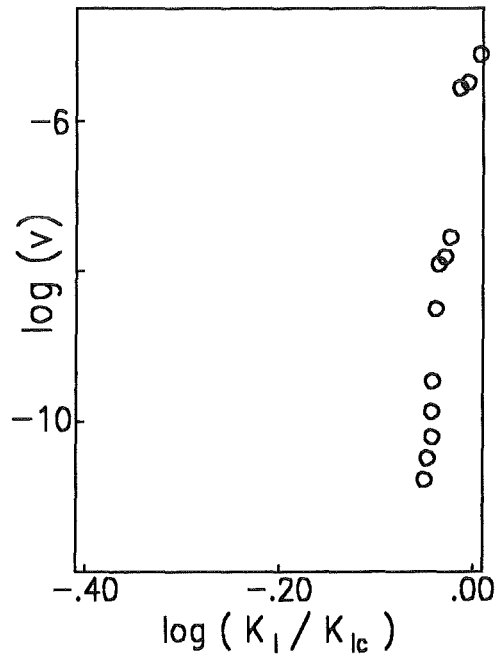


Figure 36. . v-K-curve for material XII, measured in fluoro-carbon FC43 at 50°C.

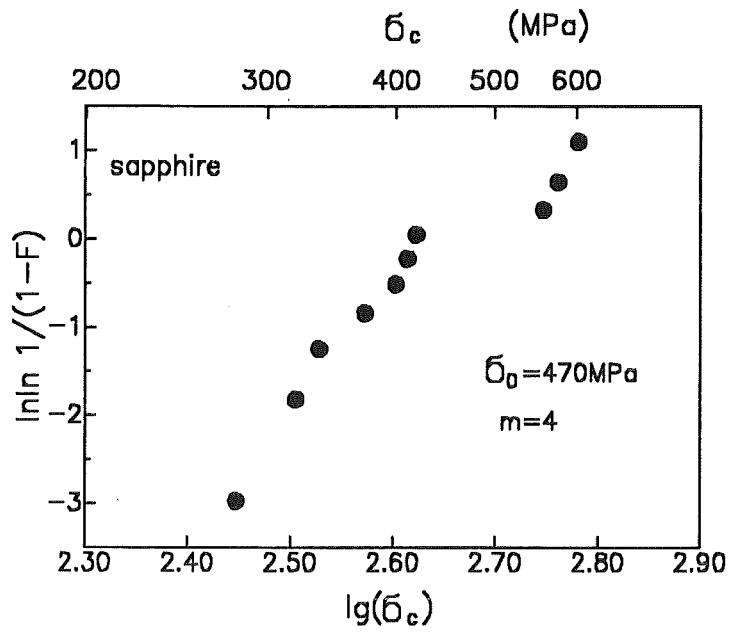


Figure 37. . Weibull-representation of bending strength (material XIII); bending bars cut out of a sapphire disc (type HEMEX). It should be noted that in these tests the cutting procedure may affect the strength unfavourably. This was the reason to perform ring-on-ring tests (see next figures).

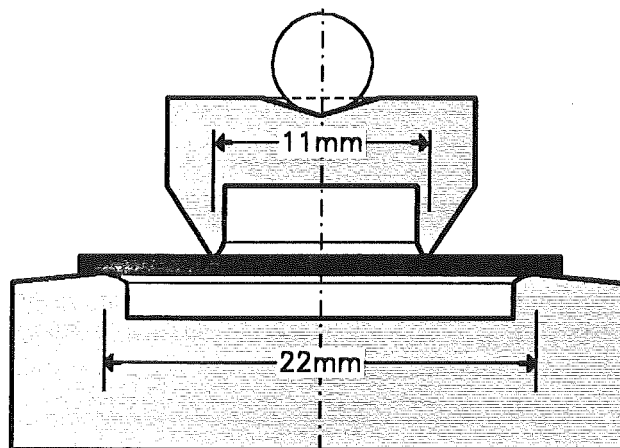


Figure 38. . Testing device for ring-on-ring tests.

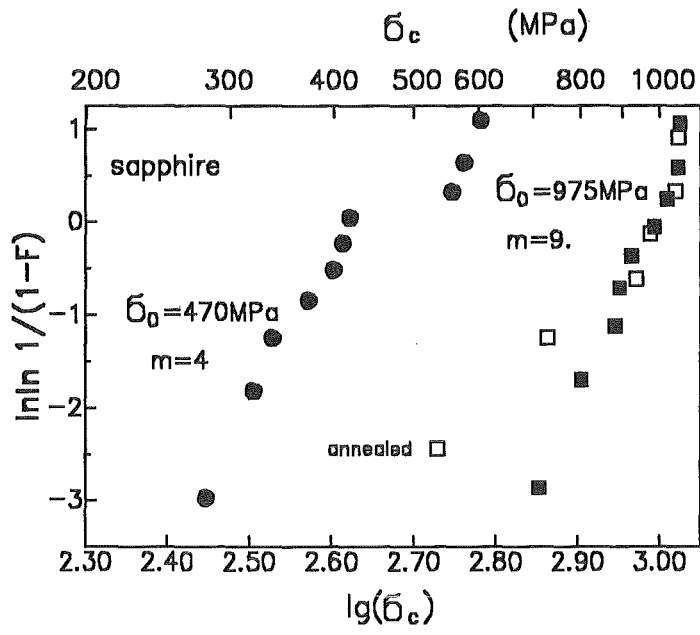


Figure 39. . Weibull-representation of bending strength (material XIII); ring-on-ring tests (squares), open squares: specimens annealed before testing.

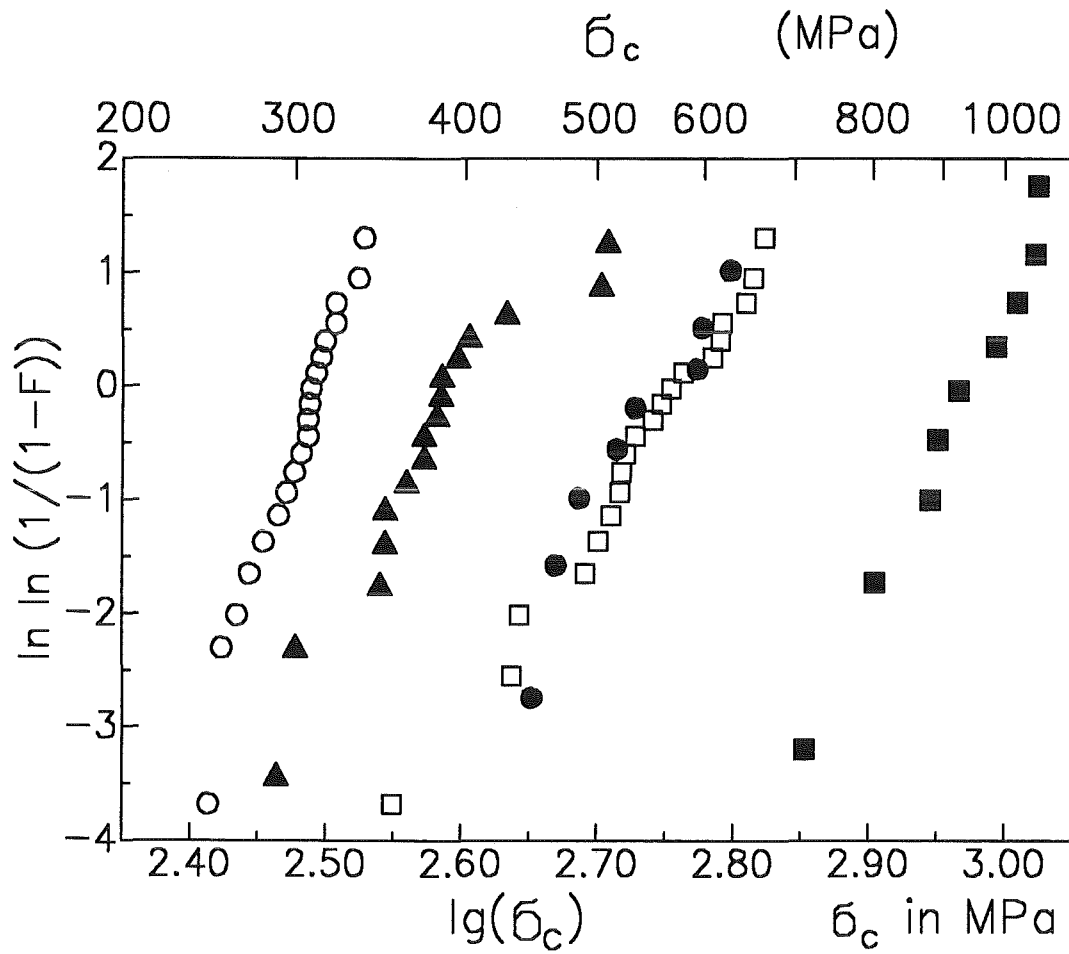


Figure 40. Comparison of first choice materials for HF-windows. Weibull-representation of bending strengths for materials I and X-XIII:
 triangles: material I, solid circles: material X, open squares: material XI, open circles: material XII, solid squares: material XIII.

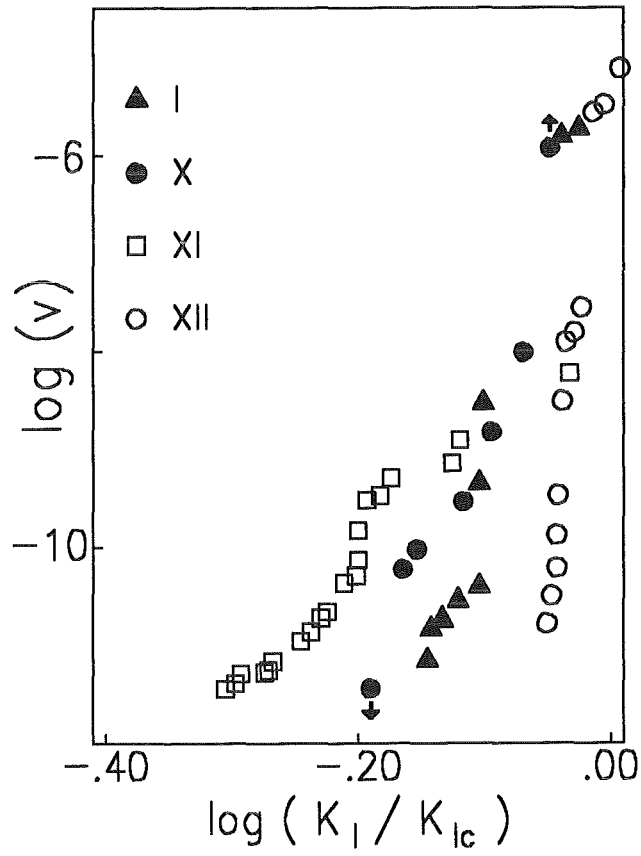


Figure 41. Comparison of first-choice materials for HF-windows. v-K-curves for materials I and X-XII.